Gas-Phase Transport during the Spreading of MoO_3 on Al_2O_3 Support Surfaces: Photoelectron Spectromicroscopic Study†

S. Günther

Institut für Physikalische Chemie und Elektrochemie, Universität Hannover, Callinstrasse 3-3a, 30167 Hannover, Germany

F. Esch

TASC Laboratory, Area Science Park, 34012 Trieste, Italy

L. Gregoratti, A. Barinov, and M. Kiskinova

Sincrotrone Trieste, Area Science Park, 34012 Trieste, Italy

E. Taglauer

Max-Planck-Institut für Plasmaphysik, EURATOM Association, Boltzmannstrasse 2, 85748 Garching, Germany

H. Knözinger*

Department Chemie, Ludwig-Maximilians-Universität München, Butenandtstrasse 5-13, 81377 München, Germany

Received: December 17, 2003; In Final Form: March 5, 2004

The spreading of MoO_3 crystallites on a flat Al_2O_3 support has been investigated by means of integrative X-ray photoelectron spectroscopy and laterally resolving photoelectron spectromicroscopy. The effect of different heat treatments on the spreading of the MoO_3 crystallites has been studied by systematically varying the temperature, the total pressure, and the humidity of the oxygen atmosphere. The chemical images and the quantitative analysis of the lateral expansion of the spread phase around a single MoO_3 crystallite provided insight in the effect of the parameter changes, since the same crystallite could be monitored and the spread layer was removed prior to each heat treatment. The obtained data set strongly supports that gas-phase transport is responsible for the spreading and wetting of molybdate species on the support surface. A model is discussed that consistently explains all experimental observations.

1. Introduction

The spreading of an active catalyst component on a support material is one of the important processes during catalyst preparation.[1] In typical monolayer-type catalysts the active phase consists of a metal oxide dispersed on a metal oxide support.[2,3] Alumina-supported Mo oxide catalysts belong to this class of catalysts.[4−9] The spreading and wetting of MoO_3 on Al_2O_3 has been extensively studied during the last two decades.[10−14] It was shown that upon annealing in oxygen or in air MoO_3 completely wets the Al_2O_3 support. When water is present in the gas phase during annealing, spreading takes place much faster than in a dry atmosphere, leading to a monolayer (1 ML) of a polymolybdate phase on the support surface.[10] The MoO_3 exceeding 1 ML loading remains in the crystalline structure.[4,7] If, on the other hand, annealing is carried out in dry oxygen, spreading takes place as well but the wetting phase consists of poorly crystalline MoO_3.[13] This surface phase is extremely sensitive to humidity. Already at room temperature the transformation of this phase into a polymolybdate layer was detected when water vapor was introduced in the gas ambient.[12,13] It was furthermore shown that this solid wetting preparation route yields a catalyst that has catalytic properties for thiophene hydrodesulfurization comparable to those of catalysts prepared by impregnation techniques.[15] Although this system is well-characterized, the active transport mechanism that accounts for the spreading is still unknown. Since no gas-phase species were detected during spreading by Raman spectroscopy[13] and since only a small effect of the gas flow direction was detected in two-bed reactor studies,[9,16] it was concluded that gas-phase transport seemed to be unlikely. On the other hand, the transport of molybdates in the millimeter to centimeter range was detected by Raman microscopy.[17] On the basis of these results it was concluded that a so-called unrolling carpet mechanism most likely accounts for the transport process. It should be noted that all these experiments were performed with mixtures of MoO_3 and Al_2O_3 powders. This fact questions several assumptions on the nature of the gas flow in the above-mentioned investigations. Therefore photoelectron spectromicroscopy studies were performed, which use MoO_3 crystallites on a flat Al_2O_3 support as model samples.[18,19] The combination of the simplified geometry and the high surface sensitivity of the method enabled for the first time direct imaging of the initial steps during spreading.[19]

† Part of the special issue "Gerhard Ertl Festschrift".

* Author to whom correspondence should be addressed. E-mail: helmut.knoezinger@cup.uni-muenchen.de.

10.1021/jp031333w CCC: $27.50
Published on Web 05/28/2004

The results of these spectromicroscopic studies questioned the role of the unrolling carpet mechanism. In the present work systematic studies were performed by integrative and spatially resolved X-ray photoelectron spectroscopy (XPS). The results strongly suggest that in fact gas-phase transport accounts for the spreading of MoO_3 on the Al_2O_3 support.

2. Experimental Section

The experiments were performed on a conventional laboratory XPS (ESCA system Phi 5600) and the scanning photoelectron microscope (SPEM) at the ELETTRA synchrotron radiation source.[20] In the SPEM the monochromatized photon beam is demagnified to a small spot by use of zone plate optics. The emitted photoelectrons are collected by a 100 mm hemispherical analyzer. The analyzer entrance lens is mounted at 70° with respect to the sample normal and its acceptance angle is ±15°. The microscope can work either in μ-spectroscopy, acquiring the energy distribution curve of the electrons emitted from the illuminated spot of the surface, or in the imaging mode. In the latter mode the sample is mechanically scanned in front of the illuminating spot while photoelectrons are collected with a chosen kinetic energy, for example, adjusting the energy acceptance to the emission from a certain core or valence level.[20,21] When core-level photoelectrons are collected, the contrast of the image reflects the lateral variations in the chemical composition of the sample.[22] The detailed procedure for obtaining a chemical map of the imaged surface was reported earlier.[22,23] The SPEM experiments were carried out with a photon energy of 590 eV, lateral resolution of 0.15 μm, and an energy resolution of ~0.4 eV in the μ-spectroscopy mode.

As a support we used a high-purity Al foil mechanically mirror-polished and subsequently anodically oxidized following a recipe described elsewhere.[24,25] Subsequent heat treatment of the oxidized Al foil at 823 K for 4 h in oxygen transformed the amorphous oxide layer into a polycrystalline γ-Al_2O_3 film of approximately 20 nm thickness. The use of this thin oxide film as support reduced the charging by the focused X-ray beam to about 2 eV, which ensured reproducible imaging and μ-spectroscopy.[18] The model surface was prepared by placing small MoO_3 crystallites on the flat support foil, using a drop of a suspension of MoO_3 crystallites in methanol released on the support with the help of a pipet. The methanol evaporated nearly instantaneously, and spatially well-separated MoO_3 crystallites remained on the surface as verified by optical microscopy. For the conventional, integrative XPS measurements a drop covering the hole sample was released from an ordinary pipet, while for the SPEM experiments a micropipet was used to place a small drop of the suspension on the surface that restricted the MoO_3 loaded area to <1 mm^2. Close to the edge of the evaporated drop one finds well-separated MoO_3 crystallites surrounded by a radius of several hundred micrometers of free Al_2O_3 support surface. In the SPEM experiments the spreading of MoO_3 released from a single crystallite could be monitored, following systematically the effect of different sample treatments. The samples were treated ex situ in a separate glass reactor, where they could be heated in dry or humid oxygen with an adjustable pressure and gas flow. A typical gas flow was 10−20 L/h, and the total pressure was varied between 1 bar and 1 mbar. For the conventional XPS measurements a special preparation setup was used, which will be described in the next section.

3. Results and Discussion

3.1. Conventional XPS Measurements. The questions arising from the observed molybdena gradients on the alumina support about the validity of the unrolling carpet mechanism suggested that the gas-phase transport should be again considered as a potential transport mechanism.[19] To verify that transport of MoO_3 through the gas phase takes place, the following experimental procedure was used. First, a MoO_3-loaded Al_2O_3 support foil was heated to 670 K in oxygen at 1000 mbar until complete spreading of MoO_3 occurred. Similar to the results reported in refs 7 and 18, the increase of the Mo 3d intensity of the sample after the heating procedure can be interpreted as the wetting of the support foil by material released from the MoO_3 crystallites. After the annealing procedure the sample consists of the spread phase wetting the Al_2O_3 support and MoO_3 crystallites on top of the support foil. Then a second Al foil (with its natural surface oxide) was placed at a distance of ~300 μm facing the MoO_3-loaded spread sample. This was achieved by placing the MoO_3-loaded sample and the Al foil in a cut glass tube as shown in Figure 1. The glass tube was transferred into the reactor, where both samples were heated in a flow of dry oxygen. After each heating step (at different oxygen pressures and annealing temperatures) the initially Mo-free Al foil facing the MoO_3-loaded sample was analyzed by integrative XPS. Since the two samples did not touch each other, an appearance of a Mo 3d signal on the Al foil should confirm the presence of a gas-phase transport, as described below. Moreover, if the pressure during the heat treatment is reduced substantially, the increase of the mean free path length of the released molecules in the gas phase should result in an increase of the amount of Mo material on the Al foil. This assumption is based on a simple scenario of the gas-phase transport. Some molecules, released into the gas phase from MoO_3 crystallites during heating, can collide with oxygen molecules while travelling through the gas phase, resulting in a change of their initial trajectory. Subsequent scattering events can result in returning of some of the released particles back to the support foil where they can stick or re-evaporate. When the pressure is sufficiently reduced, the initial flight direction of the released molecules is not (or is less) affected and more material should be transported toward the Al foil opposite the MoO_3-loaded sample. Since the MoO_3 trimers are the most prominent species in MoO_3 vapor at ~700 K,[26,27] we consider $(MoO_3)_3$ and MoO_3 molecules for the estimation of the mean free path length in the O_2 atmosphere. The mean free path of the released molecules [with $m(MoO_3) = 144$ amu or $m[(MoO_3)_3] = 432$ amu] in the O_2 gas phase [with $m(O_2) = 32$ amu] can be calculated with the assumption of collisions of hard spheres. Within this assumption, the cross section σ_S can be approximated as $\sigma_S = \pi (r_1 + r_2)^2$ with r_1 (O_2) = 1.2 Å and $r_2 = 1.9$ or 3.9 Å for the monomer or trimer, respectively. These numbers give at 670 K and 1 bar oxygen pressure a mean free path length, l, of 0.03−0.1 μm. At 4 mbar l raises up to 10−30 μm, which means that the evaporated molecules experience several tens of collisions on their way through the 300 μm gap between the two foils.

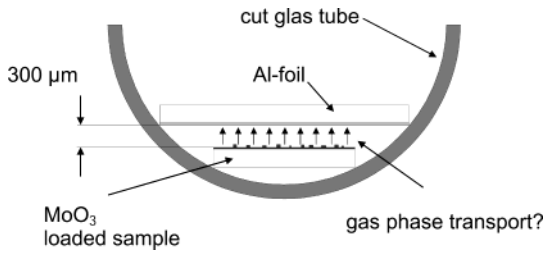

Figure 1. Schematic representation of the setup used to monitor transport of molybdate species through the gas phase during heat treatments by integrative XPS. The gap between the Al foil and the MoO_3-loaded sample placed in the cut glass tube is about 300 μm.

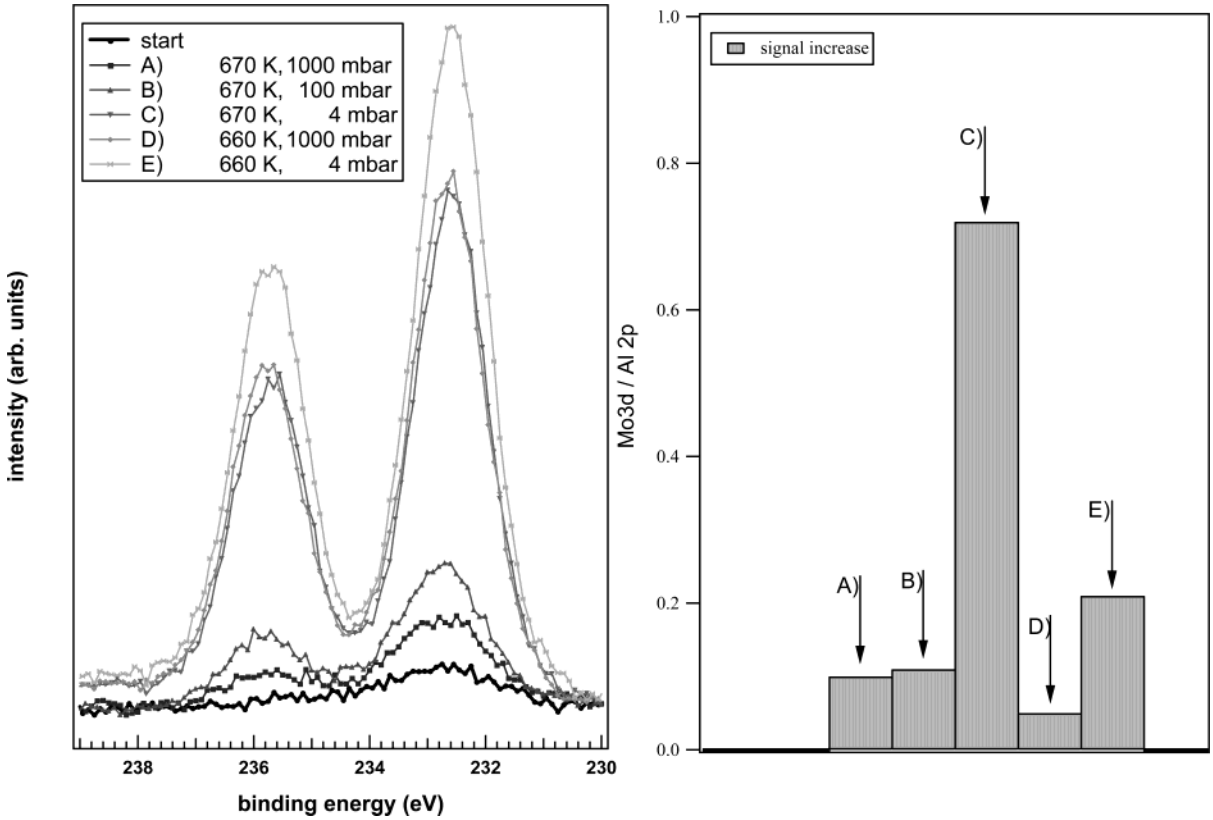

Figure 2. Integrative XPS results obtained from the Al foil in the setup shown in Figure 1 after following annealing steps in dry oxygen for 40 min: (A) 670 K, 1000 mbar; (B) 670 K, 100 mbar; (C) 670 K, 4 mbar; (D) 660 K, 1000 mbar; (E) 660 K, 4 mbar. The left panel displays the Mo 3d spectra normalized to the corresponding Al 2p spectra. The right panel shows the relative increase of the Mo 3d/Al 2p intensity ratio after each annealing step.

Thus, at $p \leq 4$ mbar an enhanced transport of the released material to the opposite Al foil should be expected. Figure 2 shows that this is indeed the case. The left panel illustrates the Mo 3d spectra measured on the Al foil after each treatment step scaled to the corresponding Al 2p peak in order to be comparable. The right panel displays the signal increase of the corresponding Mo 3d/Al 2p intensity ratio of the spectra obtained after each successive treatment step. It is clearly visible that already after the first heat treatment at 670 K in dry oxygen at 1 bar (A) a Mo 3d signal is detectable on the surface of the Al foil facing the MoO_3-loaded sample, which can be a result only of transport through the gas phase. While the Mo 3d/Al 2p signal increase at $p = 100$ mbar (B) equals the one at 1 bar (A), the increase becomes pronounced when the sample is annealed at 4 mbar (C). The same trend is visible at a lower level when the annealing temperature is reduced to 660 K at 1 bar (D) and at 4 mbar (E).

In separate experiments it was also determined that such Mo 3d spectra were not seen when a clean Al foil was heated in the empty glass reactor, which confirms that the Mo particles were not stored and/or released from the reactor walls. Furthermore, it was shown that an already Mo oxide-covered Al foil (e.g., the one from step C in Figure 2) did not lose its Mo 3d signal after heating to 660 K in the empty reactor, which means that the Al foil did not re-evaporate the adsorbed molybdate phase during heating. Thus, the Mo 3d intensity of the Al foil opposite the MoO_3-loaded sample represents a good monitoring signal for the amount of material that was transported through the gas phase. The described experiments clearly demonstrate that gas-phase transport takes place during the thermal treatment and that the observed effects upon variation of the oxygen pressure are consistent with the quantitative approximations made on the basis of the kinetic gas theory. It remains to be tested whether the lateral spreading on the MoO_3-loaded sample also takes place via evaporation into and readsorption from the gas phase or via surface diffusion processes.

3.2. Experiments with Laterally Resolving XPS. In the laterally resolving experiments the gradient of the released material around a single MoO_3 crystallite was measured and related to the parameters applied during the heat treatment. The experiments were performed in the following way: a specified MoO_3 crystallite was selected and the area around it was characterized in SPEM before spreading. Then the sample was annealed in the ex situ reactor and the material gradient around the MoO_3 crystallite was determined. Before the following heat treatment the spread material was removed from the Al_2O_3 support by Ar^+ sputtering in order to reach the same starting condition of the sample. In this manner we carried out several heat treatments, changing one parameter (e.g., the temperature or the gas pressure) each time in order to probe its effect on the spreading around the same MoO_3 crystal. To remove completely only the spread phase without damaging the γ-Al_2O_3 film or losing the MoO_3 crystals, the correct settings of the Ar^+ sputtering were determined in separate test experiments. (A scanning differential ion gun, model 04-303A from Perkin-Elmer, was used for sample sputtering at room temperature for 40 min at 3 keV and 0.8 μA sample current.) As mentioned above, the used preparation technique deposits a sufficient amount of isolated MoO_3 crystallites, which is of crucial importance for the success of the studies. The effects of three different parameter changes during the heat treatment were monitored, namely, (i) temperature variation from 630 to 715 K during heating in dry oxygen, (ii) pressure variation between

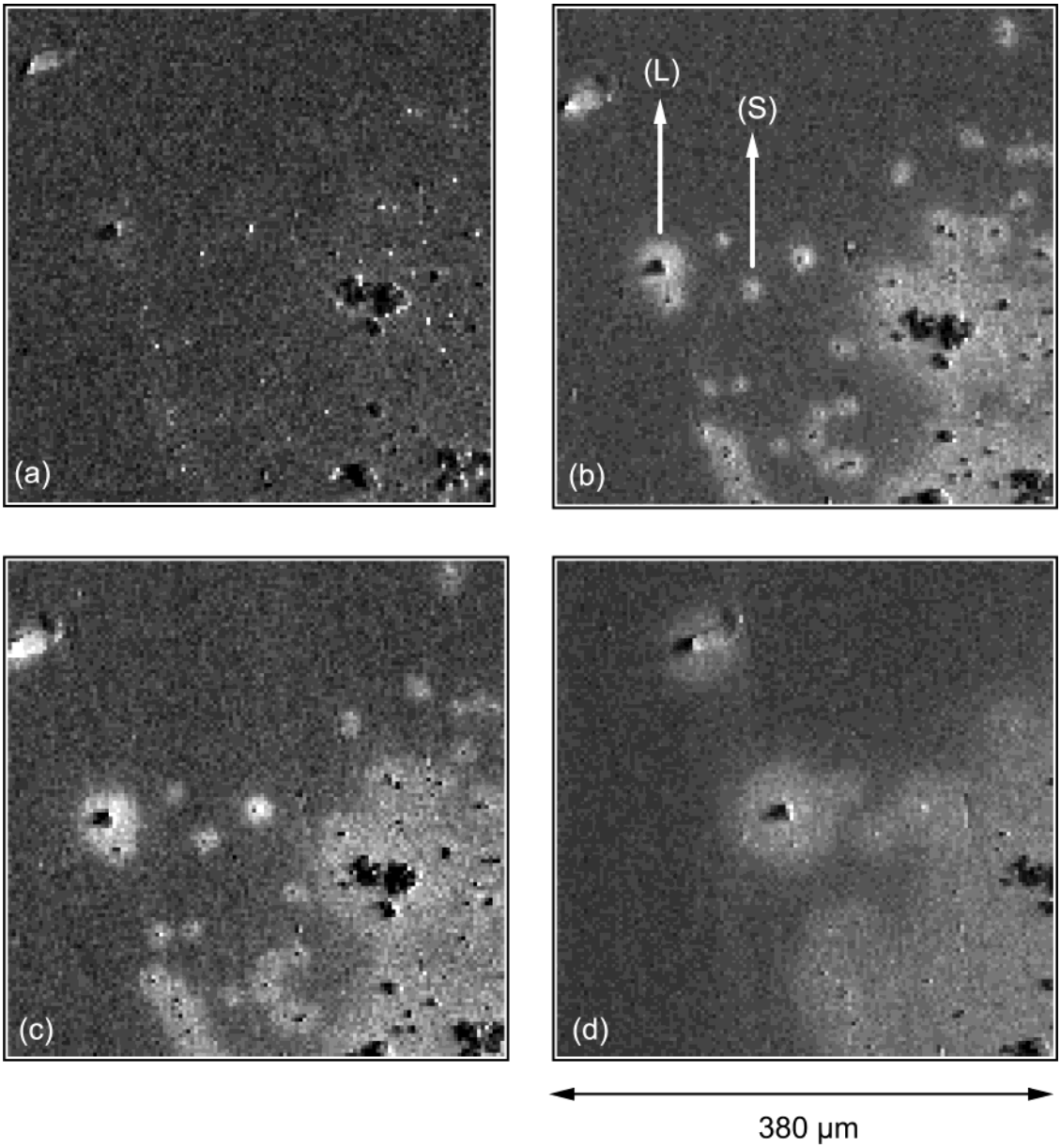

Figure 3. Mo 3d images taken before (a) and after heat treatments in dry oxygen at different temperatures (b−d). The status of the sample before each annealing step, i.e., after removal of the spread surface layer by Ar^+ sputtering, is represented by image a. The temperature treatment in dry oxygen was (b) 280 min at 630 K, (c) 60 min at 660 K, and (d) 60 min at 700 K. The arrows in image b indicate the areas above the selected large (L) and small MoO_3 crystallite (S), within which the Mo gradients displayed in Figure 4 were measured. Each image was taken by use of the Mo 3d core level emission from the spread phase (which takes place at a different energy than the emission from the MoO_3 crystallites; see, e.g., ref 19). The gray scale represents the amount of spread Mo species.

25 and 1000 mbar during heat treatment at 660 K in dry oxygen, and (iii) the addition of 32 mbar of H_2O vapor to the O_2 gas atmosphere at 1000 mbar and temperatures of 530 and 560 K.

3.2.1. Temperature Variation. Figure 3 shows Mo 3d overview images of the MoO_3-loaded area prior to and after heat treatment in dry oxygen at three different temperatures. The starting surface of each annealing experiment is always the Ar^+-sputtered sample (40 min at 3.0 kV), where the spread layer is removed as visible in the upper left image. The other images clearly demonstrate that with increasing temperature the material released from the MoO_3 crystallites increases and wets larger areas of the surrounding support surface. The arrows indicate the areas around two selected crystallites [a large (L) and a small one (S)], where the released material was measured quantitatively by μ-spectroscopy. To determine the gradient around each crystallite the X-ray beam was subsequently stepped along the indicated arrow. At each step the distance to the crystallite center and the Al 2p and the Mo 3d spectra were measured. From the corresponding intensities $I_{Al\ 2p}$ and $I_{Mo\ 3d}$, the Mo coverage θ_{Mo} can be determined by calculating the ratio $\theta_{Mo} = 1/0.11 \times I_{Mo\ 3d}/[I_{Mo\ 3d} + SI_{Al\ 2p}]$ with $S = 9$, following the calibration procedure described elsewhere.[19] Note that due to the different analyzer setting during the measurements of the discussed data the sensitivity factor S is slightly changed with respect to the one used in ref 19. Figure 4 shows the resulting plots for the measured coverage versus the distance from the center of the MoO_3 crystallites. It is clear that the small crystallite releases less material (note the different x-axis scaling), but the gradients have similar shapes. Especially the occurrence of a plateau in the gradient after reaching 1 ML clearly manifests that indeed the spread layer consists of a single wetting layer. In ref 19 it has been shown that the material release can be approximated by a point-source model with a central source emitting q particles per second (or ML μm^2/min),

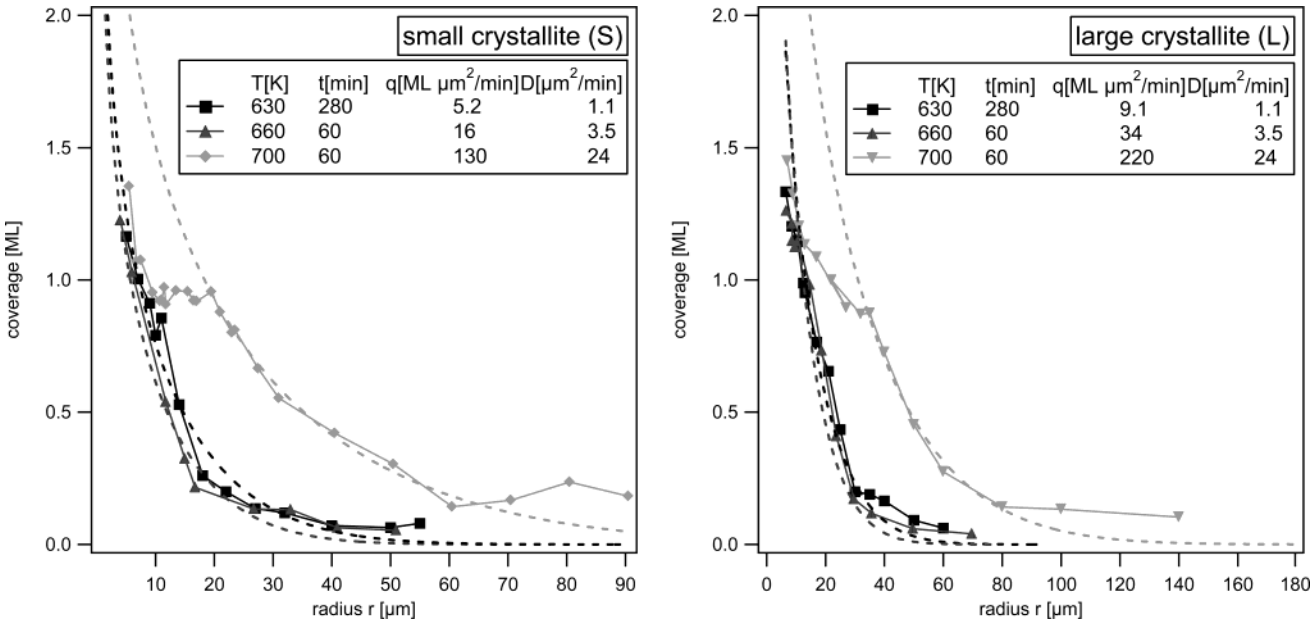

Figure 4. Mo gradients obtained by μ-spectroscopy around the small (S) and the large MoO_3 crystallite (L), indicated in Figure 3b, after annealing in dry oxygen at different temperatures. The dashed lines are fits of the point-source solution to the experimental data.

which diffuse with a diffusion constant D (in square centimeters per second or square micrometers per minute). The solution to this problem is

$$N(r,t) = q/4\pi D \int_{r^2/4Dt}^{\infty} \frac{\exp(-x)}{x}\,dx$$

The dashed curves in Figure 4 are fits to this solution. In the case of a plateau we decided to use the part of the gradient where the Mo coverage is lower than 1 ML, since saturation above 1 ML is not included in the model. The obtained values for q represent an upper limit for the correct value, whereas the ones for D are a lower limit. The error due to this simplification is small, although the discrepancy between the experimental and the fitted data is well visible; for example, the overestimation of q by the point-source model is less than 15% (note that the emitted material is calculated by $2\pi\int\theta r\,dr$ and that therefore the deviation of θ for small r does not contribute much).

Table 1 lists the obtained parameters for q and D for the fitted data from Figure 4. Assuming that

$$D = D_0 \exp(-E_{d1}/kT)$$

and

$$q = q_0 \exp(-E_{d2}/kT)$$

are valid, one can determine D_0 and q_0 and the energy barrier E_d for the corresponding process. These values are also listed in Table 1. It is clear that the data for D_0 and q_0 and the corresponding E_d are not very precise since only a limited temperature interval can be covered by the measurements. Nevertheless, these values can be used to discuss the order of magnitude effects as will be done in the following.

Assuming a surface diffusion process, an upper limit of the diffusion constant D can be approximated by the tracer diffusion constant $D = g^2\nu \exp(-E_{d1}/kT)$, where the jump length g equals the distance to the next-neighbor site of $\sim$4 Å and ν equals the typical attempt frequency of $\sim 10^{12}$ s^{-1}. With these numbers one obtains a value for $D_0 \sim 1.6 \times 10^{-3}$ cm^2/s. Comparison with the experimental values in Table 1 shows that this value is 10^6-10^7 times too small. Therefore a simple surface diffusion mechanism seems to be very unlikely.

TABLE 1: Values of q and D from the Fits of the Point-Source Solution to the Experimental Data of Figure 4[a]

	small crystal (S)		large crystal (L)	
temperature (K)	q (ML μm^2/min)	D (μm^2/min)	q (ML μm^2/min)	D (μm^2/min)
630	5.2	1.1	9.1	1.1
660	16	3.5	34	3.5
700	130	24	220	24
q_0, D_0	5.8×10^{14}	4.3×10^{13}	9.6×10^{14}	4.3×10^{13}
q_0 (particles/s)[b]	9.6×10^{19}		1.5×10^{20}	
D_0 (cm^2/s)		7.2×10^3		7.2×10^3
E_d (eV)	1.77	1.70	1.77	1.70

[a] The corresponding values of q_0, D_0, and E_d were calculated with the assumption of Arrhenius behavior. [b] A surface packing density of 9.9×10^6 sites/μm^2 for γ-Al_2O_3 is assumed.

On the other hand, one can assume a gas-phase transport mechanism of the following scenario: a molecule is evaporated from the MoO_3 crystal into the gas phase, where it moves with isothermal velocity until it collides with an O_2 molecule, resulting in a change of its trajectory. By chance it can hit the support surface, where it sticks and contributes to the spread phase. In this model the jump length g equals the effective distance from the evaporation site to the place, where the molecule first hits the support surface. By re-evaporation from the support the molecules can again enter into the gas phase and perform another effective jump toward the next adsorption site on the support, which leads to the diffusion-driven wetting of the substrate. In this model E_{d1} and E_{d2} equal the activation barrier for the evaporation from the MoO_3 crystal and the re-evaporation from the support surface, respectively. The order of magnitude of the effective jump length was approximated by a simple hard-sphere model for a $(MoO_3)_3$ molecule in an O_2 gas atmosphere. The molecule is evaporated from a point source at the origin of the coordinate system into the gas phase, where it performs a random walk-type motion. After each mean free path it collides with an O_2 molecule and its new flight direction is calculated with the assumption of an elastic collision of hard spheres. (The model neglects the rotational motion of

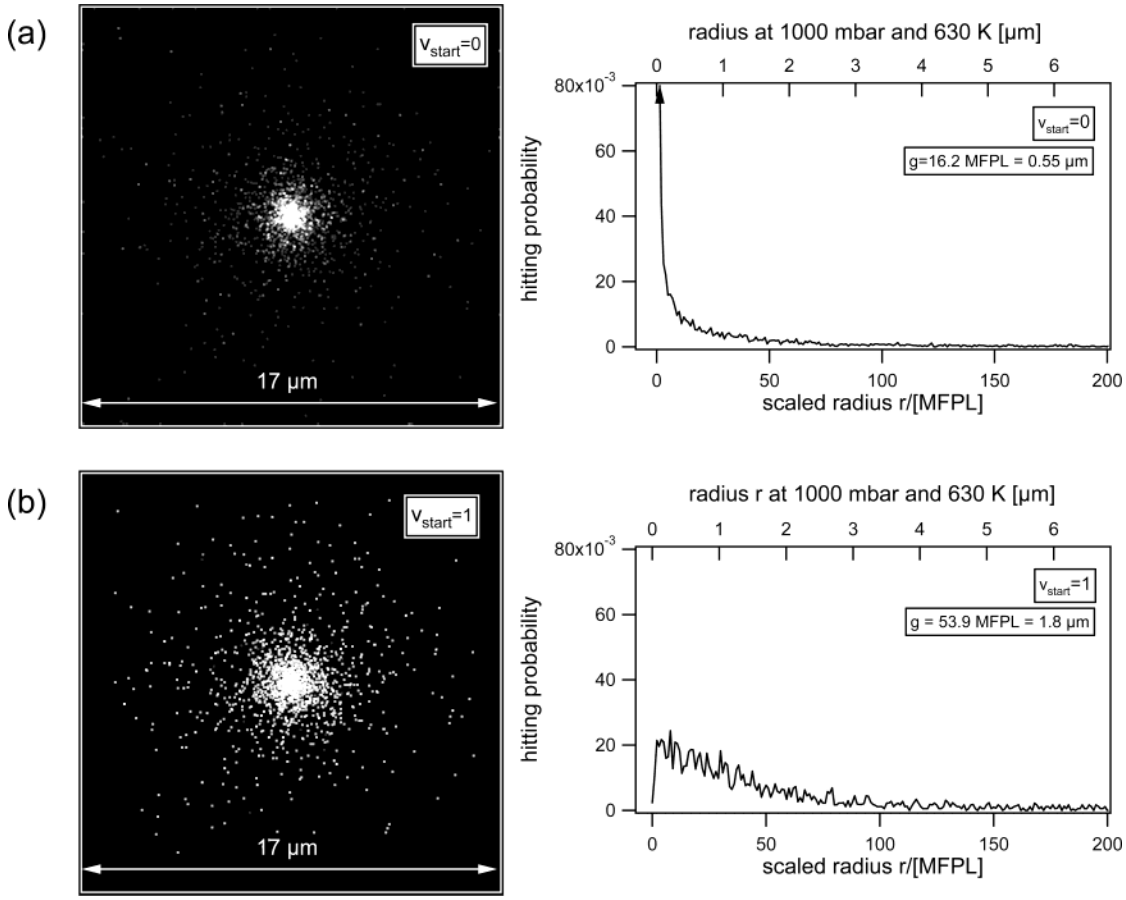

Figure 5. Positions at which $(MoO_3)_3$ molecules, emitted from a point source in the image center, hit back the support surface after being scattered by O_2 molecules in the gas phase, calculated with a hard-sphere approximation. The distributions for an evaporation direction perpendicular to the surface were calculated. Two extreme cases of the initial velocity of the emitted molecules ($\upsilon_{start} = 1$ and $\upsilon_{start} = 0$) for an oxygen atmosphere of 1000 mbar at 630 K are considered and shown in panels a and b, respectively. The images use a comparable gray scale, where the number of hits correspond to the gray level of the spot. The resulting distributions are displayed beside each image. Here, the lower *x*-axis indicates the distance in units of the mean free path length, whereas in the upper *x*-axis these numbers are converted in micrometers, the scale also used in the corresponding images and the indicated effective displacement $g = \int r\, P(r)\, dr$.

the corresponding molecules.) The motion of the scattered molecule is calculated until it hits the support surface. The distance of this position from the origin is stored. Thus, the probability $P(r)$ to find the $(MoO_3)_3$ molecule at a distance r from the point source can be calculated. Here, the evaporation direction and the initial velocity of the evaporated molecule are crucial parameters for the resulting distribution $P(r)$ and the corresponding value for g. Since the angular distribution of the evaporation process is unknown, we restricted the discussion to evaporation perpendicular to the surface in order to keep the simulation model simple. Concerning the initial velocity, two extreme cases were considered: in the first case, the $(MoO_3)_3$ molecule is evaporated with its mean thermal velocity perpendicular to the surface ($\upsilon_{start} = 1$), while in the other case the molecule is in rest position ($\upsilon_{start} = 0$) and picks up the velocity by the collision with the O_2 molecules. The calculated positions where the $(MoO_3)_3$ molecules land on the surface and the corresponding probability distribution $P(r)$ for these two cases are displayed in Figure 5. From the distribution $P(r)$, the mean displacement g from the origin is obtained via $g = \int r\, P(r)\, dr$. It ranges between 16 and 54 mean free path lengths, depending on υ_{start}. At 670 K and 1 bar this corresponds to a value for the effective displacement g between 0.5 and 1.8 μm. In this case, the effective displacement g is about 10^3-10^4 times greater than an atomic distance, so that the calculated values for D_0 agree well with the experimental data. Although it is reported that the $(MoO_3)_3$ molecule is the most prominent species in the MoO_3 vapor,[26,27] the distribution $P(r)$ has also been calculated for a diffusing MoO_3 molecule, since it is a priori not known which molecular species is present in the gas phase during the spreading process. The calculated mean displacement of the MoO_3 molecule is very similar to the one obtained for the trimer since the two effects nearly cancel each other. On one hand, the mean free path of the MoO_3 molecules is larger than that of the trimer (higher thermal velocity); on the other hand, the MoO_3 molecules require less collisions with the O_2 molecules in order to be redirected to the support surface (higher mass of the trimer). The values of the effective displacement g, calculated above, can be regarded as a good order of magnitude approximation of the described gas-phase transport, because the results are not affected too much by the details of the assumed gas-phase process.

It should be noted that the above model can only be used to analyze the initial stage of the spreading process. The fact that the gradient shows a plateau above 1 ML coverage and that the completely spread phase does not exceed 1 ML implies that in the gas-phase model a molecule hitting an already spread layer does not stick and is immediately re-evaporated. This means that the activation barrier becomes coverage-dependent (it approaches zero for $\theta = 1$ ML) and that the diffusion coefficient D increases with the amount of the already wet surface. In this case, D cannot anymore be regarded as a constant and the applicability of the point source solution described above is no longer valid. Therefore, the above discussion yields a good

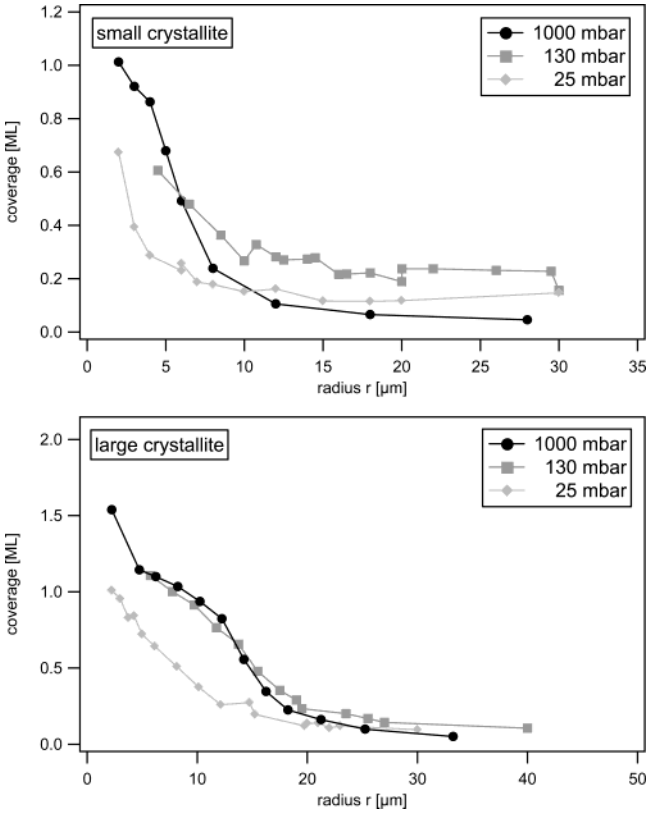

Figure 6. Effect of the pressure variation on the Mo gradient around a small (upper panel) and a large MoO_3 crystal (lower panel). The annealing was performed at 660 K in dry oxygen.

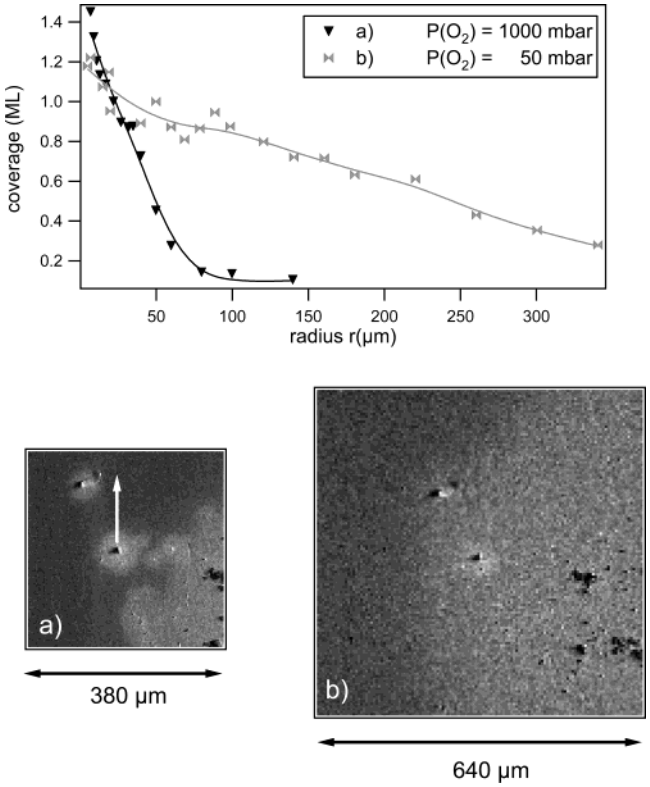

Figure 7. Material gradients of the same area of the sample around the central crystallite and the corresponding images, measured after two successive heat treatments in dry oxygen at 700 K for 60 min at (a) 1000 mbar and (b) 50 mbar. Before each experiment the spread layer of the starting surface was removed by sputtering. Clearly, an increased transport over several hundred micrometers upon lowering the pressure is verified. The displayed gray scale represents the amount of released Mo species covering the support.

estimation only during the initial stage of the spreading, where only a small part of the support surface is wet.

The values for the rate of the released material q can be related to the available desorption sites N of the corresponding emitting MoO_3 crystallites. The preexponential term q_0 equals the available desorption sites of the crystallite N times the attempt frequency ν, i.e., $q_0 = N\nu$. According to Table 1 the rate q_0 is $1-2 \times 10^{20}$ particles/s. Assuming $\nu = 10^{12}$ s^{-1}, we obtain $N = (1-2) \times 10^8$ particles. Taking into account the packing density of MoO_3 of 1.4×10^7 particles/μm^2, this equals an active surface of about 3×3 μm^2. This value equals roughly the dimension of the investigated crystallites. Thus, the order of magnitude seems to be consistent with the gas-phase model, in which the crystallite evaporates material from its surface. It should be noted that the latter approximation only states no contradiction with the proposed gas-phase model, since the actual surface area of the investigated MoO_3 crystallites is unknown and most probably exceeds the overall crystal dimension due to their irregular and porous morphology.

3.2.2. Pressure Variation. The experiments described in this section involve samples annealed in dry oxygen (10−20 L/h) for 60 min at 660 K and pressures varying from 25 until 1000 mbar. The material gradient around an emitting MoO_3 crystal should be sensitive to the O_2 pressure if the transport takes place through the gas phase but not in the case of surface diffusion. In the case of gas-phase transport the released material should distribute on a wider area, lowering the pressure, since the mean free path length in the gas phase is increased. Therefore, at low pressure the Mo coverage of the spread phase should be smaller in the vicinity of the MoO_3 crystallite, whereas the material gradient should expand at larger distance, as is manifested by the experimental results shown in Figure 6. Here, two different MoO_3 crystals (again a small and a large one) were monitored before and after spreading in dry oxygen at 1000 and 25 mbar. It is clearly visible that after the low-pressure treatment the coverage close to the crystallite has decreased, while at larger distances the coverage is higher than that reached after annealing at high pressure. It should be noted that one would expect a much more dramatic effect when the material gradient around a point source is considered. As can be seen in Figure 5 for the distribution around a point source, the r-axis scales with the mean free path length of the molecule in the gas phase, which is inversely proportional to the pressure. Therefore, when the pressure is lowered by a factor of ∼30, the r-axis should increase by this factor and the hitting probability should drop by the order of $1/(30)^2 \approx 1/1000$. Accordingly, one would expect such a reduction of the coverage in Figure 6. This is not observed experimentally, because the emitting MoO_3 crystallite is not a point source. In fact, its lateral dimensions are independent of the mean free path length and therefore the material distribution close to the crystallite does not scale with the pressure. Qualitatively this can be seen directly if one considers a molecule that is emitted from an extended object in a direction facing the support surface. As long as the mean free path length is small relative to the height of the emission point, the position at which the emitted molecule finally hits the support is determined by the random walk in the gas phase. If, on the other hand, the mean free path length exceeds the height above the surface, the emitted particle travels toward the surface without colliding with a gas-phase molecule, i.e., the position where it hits the support does not depend on the pressure of the gas atmosphere. The portion of material, which leaves a spatially extended object and hits the support in its vicinity

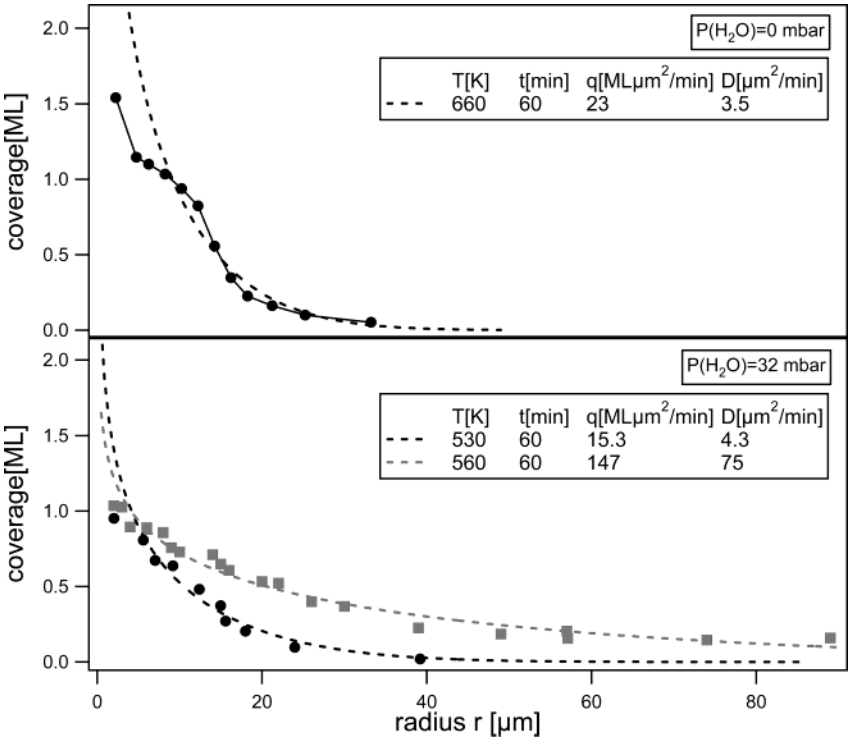

Figure 8. Mo gradients around the same MoO_3 crystallite measured (top panel) after annealing at 1000 mbar, 660 K, for 60 min in dry oxygen and (lower panel) after annealing at 1000 mbar, 530 and 560 K, for 60 min in humid oxygen with $P(H_2O) = 32$ mbar. The dashed lines are fits to the point-source solution. The indicated values for q and D reflect the enhancement of the spreading due to the presence of water.

without many collisions in the gas phase, contributes considerably to the material gradient around the crystal, if the mean free path length exceeds the object dimensions and accounts for the less dramatic effect in the gradient in Figure 6. This effect has also been tested qualitatively with the hard-sphere model described above. Since furthermore a spatially extended source acts as an obstacle for a diffusing molecule, its surface represents a reflective boundary (adsorption/re-evaporation), which also changes the shape of the material gradient in the close vicinity of the emitting object.

When the mean free path length is increased by lowering the pressure, material contributions from other emitting crystallites that are situated too close to the investigated area should also be considered. This contribution becomes even more pronounced when the support is already covered by approximately 1 ML of spread phase and the effective diffusion coefficient becomes large. In this case a dramatic influence of the pressure reduction on the amount of the wet surface is seen. Figure 7 shows such an example. First, the area of Figure 7a was imaged after heat treatment at 700 K for 60 min at 1000 mbar. It is well visible that the gradient around the central crystallite mainly originates from material that is released from this crystallite. On the support surface near the right edge of the image, the MoO_3 crystallite density is so high that a homogeneous spread phase has already developed. After removal of the spread layer by sputtering, the annealing at 700 K was repeated for 60 min at 50 mbar. The resulting image in Figure 7b shows that now the spread layer covers a much larger part of the support surface. Especially the material released from the highly MoO_3-loaded region in the right part of the image contributes to the gradient around the center crystallite as quantitatively demonstrated by the coverage versus distance plot in the top panel of Figure 7. The obvious plateau in the gradient curve at 1 ML again confirms the monolayer type of the spread layer. In brief, also the pressure experiments strongly support the gas-phase transport mechanism during spreading.

3.2.3. Effect of the H_2O Partial Pressure. In these experiments we compare the spreading of a single MoO_3 crystallite after annealing for 60 min at 660 K in dry oxygen or in oxygen containing 32 mbar of H_2O vapor. Figure 8 shows the corresponding gradient curves. The bottom panel displays the results obtained after annealing in humid oxygen. When annealing in humid oxygen, the temperature had to be lowered by ≥ 100 K in order to obtain a similar degree of spreading. The dashed lines are fits for the point-source model. The indicated values for q and D suggest that the rate of release of material from the MoO_3 crystallite and the diffusion coefficient are strongly increased in the presence of H_2O vapor. In the frame of the gas-phase transport model it means that the humidity promotes the desorption from the MoO_3 crystallite and from the spread layer. The increased rates of desorption naturally lead to a smooth gradient, which expands far away from the center of the crystallite. These findings are consistent with the gas-phase transport model, since the enhancement of the vapor pressure over MoO_3 in the presence of H_2O is a known phenomenon.[28−30]

4. Conclusions

The results of the reported experiments strongly support the conclusion that a gas-phase transport mechanism is active for the spreading of MoO_3 on a flat Al_2O_3 support under the chosen conditions. According to this mechanism, the spreading is initiated by desorption of molecular species [most probably $(MoO_3)_3$] from MoO_3 crystallites that travel in the gas phase. Collisions with the O_2 molecules in the gas phase can result in backscattering of the desorbed species onto the support surface, where they can readsorb. The sticking probability of the molecular species on an already spread layer is strongly reduced, favoring a very efficient buildup of a completely spread monolayer covering the whole support surface. This mechanism explains the efficiency of MoO_3 spreading on industrially used high-surface-area Al_2O_3 powders, which are highly porous and

expose many different surface planes and defects. Since the latter should hinder simple surface diffusion processes, the so-called unrolling carpet mechanism was favored but has been questioned recently.[19] Gas-phase transport was disregarded because (i) no gas-phase molybdate species were detected by Raman spectroscopy,[13] (ii) no influence of the gas-flow direction was found in a Raman microscopy investigation,[17] and (iii) two-bed reactor studies did not show significant transport from one catalyst bed to the next.[9,16] We believe that the very efficient way of the gas-phase transport mechanism proposed above accounts for these "negative" results. Each released molecule needs only a limited number of gas-phase collisions to return to the support surface. Therefore, the actual time period that the diffusing particle spends in the gas phase is short and the concentration of the particles in the gas phase is extremely low, i.e., below the detection limit of Raman spectroscopy. The following estimates underline this fact. From Table 1 it can be seen that the evaporation rate of the investigated MoO_3 crystallites at 660 K corresponds to $\sim 10^6$ particles/s. During the initial steps of spreading these particles undergo approximately several hundred to a thousand collisions in the gas phase, which corresponds to a time of $10^{-8}-10^{-7}$ s. Thus, the time-averaged contribution of one MoO_3 crystallite at 660 K is on the order of $10^{-2}-10^{-1}$ particles in the gas phase. The fact that the gas-flow direction had no influence on the spreading as investigated by Raman microscopy has two reasons. First, again each diffusing particle is present in the gas phase for a short period of time only and does not travel far enough from the support surface to be significantly affected by the gas flow. The second, even more important reason stems from the type of samples used in the Raman microscopy study. These were pressed pellets consisting of a mixture of MoO_3 and support powder. Because of the porous nature of these samples, the transport through the gas phase takes place nearly exclusively in the pores, where no direct gas flow is present. This fact as well as the effectiveness of the process also accounts for the negative results of the two-bed reactor studies in which powder samples were also used.

In conclusion, a simple surface diffusion mechanism for the active transport during spreading seems unlikely (see, e.g., the temperature variation data), and the unrolling carpet mechanism was already questioned.[19] In contrast, gas-phase transport was clearly evidenced by integrative XPS by the present results, and the observed gas-phase influence on the laterally resolved spreading on the support surface (see, e.g., the pressure variation data) strongly supports the presented gas-phase transport model, which consistently explains all experimental observations.

Acknowledgment. We thank Dr. C. Linsmeier for the help during the integrative XPS measurements at the Max-Planck-Institut für Plasmaphysik and D. Lonza for the excellent technical support at the ELETTRA synchrotron radiation facility. The work was financially supported by EU Contract HRPI-CT-1999-00033. S.G. thanks the Deutsche Forschungsgemeinschaft and the Sincrotrone Trieste SCpA for financial support.

References and Notes

(1) Ruckenstein, E. In *Metal−Support Interactions in Catalysis, Sintering, and Redispersion*; Stevenson, S. A., Dumesic, J. A., Baker, R. T. K., Ruckenstein, E., Eds.; Van Nostrand Reinhold Company: New York, 1987; p 230.

(2) Knözinger, H.; Taglauer, E. *Catalysis*; Royal Society of Chemistry: Cambridge, U.K., 1993; Vol. 10, p 1.

(3) Knözinger, H.; Taglauer, E. In *Handbook of Heterogeneous Catalysis*; Ertl, G., Knözinger, H., Weitkamp, J., Eds.; VCH−Verlag: Weinheim, Germany, 1997; Vol. 1, p 216.

(4) Liu, Y.; Xie, Y.; Li, C.; Zou, Z.; Tang, Y. *J. Catal.* **1984**, *5*, 234.

(5) Xie, Y.; Gui, L.; Liu, Y.; Zhao, B.; Yang, N.; Zhang, Y. G., Q.; Duan, L.; Huang, H.; Cai, X.; Tang, Y. In *Proceedings of the 8th International Congress on Catalysis, Berlin*; Dechema: Frankfurt, Germany, 1984; Vol. 5, p 147.

(6) Xie, Y.; Gui, L.; Liu, Y.; Zhang, Y.; Zhao, B.; Yang, N.; Guo, Q.; Duam, L.; Huang, H.; Cai, X.; Tang, Y. In *Adsorption and Catalysis on Oxide Surfaces*; Che, M., Bond, G. C., Eds.; Elsevier: Amsterdam, 1985; p 139.

(7) Gui, I.; Liu, Y.; Guo, Q.; Huang, H.; Tang, Y. *China Sci. B* **1985**, *6*, 509.

(8) Stampfl, S. R.; Chen, Y.; Dumesic, J. A.; Niu, C.; Hill, C. G. *J. Catal.* **1987**, *105*, 445.

(9) Leyrer, J.; Zaki, M. I.; Knözinger, H. *J. Phys. Chem.* **1986**, *90*, 4775.

(10) Leyrer, J.; Margraf, R.; Taglauer, E.; Knözinger, H. *Surf. Sci.* **1988**, *201*, 603.

(11) Margraf, R.; Leyrer, J.; Knözinger, H.; Taglauer, E. *Surf. Sci.* **1987**, *189/190*, 842.

(12) Kisfaludi, G.; Leyrer, J.; Knözinger, H.; Prins, R. *J. Catal.* **1991**, *130*, 192.

(13) Mestl, G.; Verbruggen, N. F. D.; Lange, F. C.; Tesche, B.; Knözinger, H. *Langmuir* **1996**, *12*, 1817.

(14) Hayden, T. F.; Dumesic, J. A.; Sherwood, R. D.; Baker, R. T. K. *J. Catal.* **1987**, *105*, 299.

(15) Koranyi, T. I.; Paal, Z.; Leyrer, J.; Knözinger, H. *Appl. Catal.* **1990**, *64*, L5.

(16) Leyrer, J. Spreitung und Monoschichtbildung in getragenen Oxidsystemen. Dissertation, Ludwig-Maximilians-Universität, München, Germany, 1988.

(17) Leyrer, J.; Mey, D.; Knözinger, H. *J. Catal.* **1990**, *124*, 349.

(18) Günther, S.; Marsi, M.; Kolmakov, A.; Kiskinova, M.; Noeske, M.; Taglauer, E.; Mestl, G.; Schubert, U. A.; Knözinger, H. *J. Phys. Chem. B* **1997**, *101*, 10004.

(19) Günther, S.; Gregoratti, L.; Kiskinova, M.; Taglauer, E.; Grotz, P.; Schubert, U. A.; Knözinger, H. *J. Chem. Phys.* **2000**, *112*, 5440.

(20) Casalis, L.; Jark, W.; Kiskinova, M.; Lonza, D.; Melpignano, P.; Morris, D.; Rosei, R.; Savoia, A.; Abrami, A.; Fava, C.; Furlan, P.; Pugliese, R.; Vivoda, D.; Sandrin, G.; Wei, F.-Q.; Contarini, S.; DeAngelis, L.; Gariazzo, C.; Nataletti, P.; Morrison, G. R. *Rev. Sci. Instr.* **1995**, *66*, 4870.

(21) Marsi, M.; Casalis, L.; Gregoratti, L.; Günther, S.; Kolmakov, A.; Kovac, J.; Lonza, D.; Kiskinova, M. *J. Electron Spectrosc. Relat. Phenom.* **1997**, *84*, 73.

(22) Günther, S.; Kaulich, B.; Gregoratti, L.; Kiskinova, M. *Prog. Surf. Sci.* **2002**, *70*, 187.

(23) Günther, S.; Kolmakov, A.; Kovac, J.; Kiskinova, M. *Ultramicroscopy* **1998**, *75*, 35.

(24) Linsmeier, C.; Knözinger, H.; Taglauer, E. *Surf. Sci.* **1992**, *275*, 101.

(25) Linsmeier, C. Oberflächenanalytische Untersuchungen von getragenen Rhodium-Modellkatalysatoren. Dissertation, Max-Planck-Institut für Plasmaphysik and Ludwig-Maximilians-Universität München, Germany, 1994.

(26) *Gmelin Handbuch der Anorganischen Chemie: Molybdän-Ergänzungsband Teil B1*, 8-te Auflage ed.; Springer-Verlag: Berlin, 1975; Vol. 53.

(27) Berkowitz, J.; Inghram, M. G.; Chupka, W. A. *J. Chem. Phys.* **1957**, *26*, 842.

(28) Glemser, O.; Wendland, H. G. *Adv. Inorg. Radiochem.* **1963**, *5*, 215.

(29) Glemser, O.; Wendland, H. G. *Angew. Chem.* **1973**, *75*, 949.

(30) Iorns, T. V.; Stafford, F. E. *J. Am. Chem. Soc.* **1966**, *88*, 4819.